Magnetic domain transformations in polycrystalline hard-soft giant-magnetoresistive-effect spin valves with Co-Cu-based artificial antiferromagnetic subsystems

2000 J. Phys.: Condens. Matter 12 6217

(http://iopscience.iop.org/0953-8984/12/28/318)

J. Phys.: Condens. Matter **12** (2000) 6217–6236. Printed in the UK PII: S0953-8984(00)12883-8

Magnetic domain transformations in polycrystalline hard–soft giant-magnetoresistive-effect spin valves with Co–Cu-based artificial antiferromagnetic subsystems

N Persat†‡, H A M van den Berg‡ and A Dinia‡

† IPCMS-GEMM, ULP-ECPM, CRNS-UMR 7505, 23 rue du Loess, F-67037 Strasbourg, France
‡ Siemens AG, ZT MF 1, Paul Gossen Strasse 100, D-91052 Erlangen, Germany

Received 28 March 2000, in final form 23 May 2000

Abstract. The magnetic and transport properties of hard–soft giant-magnetoresistive-effect spin valves, with a Co/Cu/Co antiferromagnetically coupled sandwich as the hard layer, are investigated. The irreversibilities in the antiferromagnetically coupled Co/Cu/Co sandwiches prepared by DC-magnetron (DC = direct current) sputtering are shown to strongly depend on the magnetic history of the samples. The irreversibilities, evidenced from analysis of the giant-magnetoresistance and magnetization responses along minor loops, are attributed to domain-phase transformations. First, the effect of the buffer stack on the structural properties and on the quality of the antiferromagnetic coupling is investigated. Coupling strengths larger than 0.4 erg cm^{-2} have been achieved for deposition on buffers containing a Cr/Fe bilayer. A method is given for estimating the amount of remanence in the Co/Cu/Co sandwich, based on the analysis of the giant-magnetoresistive response upon switching the magnetization direction of the soft magnetic layer located in the buffer. The perfect antiferromagnetic alignment at zero field is attributed to the formation of a magnetic state with relatively large domains. The small amount of remanence detected in some samples is ascribed to the persistence at zero field of a significant density of domain walls. Small fluctuations in the thickness of the layers causing a lateral distribution of the coupling strength are expected to influence the remanence magnetic state and induce differences between samples.

1. Introduction

The hard–soft systems [1–3] represent a wide category of the magnetic field sensors based on the giant-magnetoresistive (GMR) effect. These systems each contain at least one magnetic layer in the stack with a fixed orientation of the magnetization for the external field range of application. This can be achieved by taking advantage of magnetic layers with different properties. For example [1], large crystallite sizes can ensure the rigidity of the magnetization of the hard layer, while the smaller crystallites in the decoupled soft layer ensure the free magnetization's rotation upon application of an external magnetic field. Unfortunately, the combination of these properties is difficult to achieve, so an exchange-biased sensor system is preferred [2], in which an antiferromagnetic (AF) layer, like FeMn, ensures the rigidity of the biased magnetic layer via exchange anisotropy. These systems present low coercivity and high sensitivity, and are well suited for implementation in thin-film read heads. Nevertheless, the operational temperature range of these devices is limited because of the weak thermal stability of the AF layer. The recently introduced GMR sensor scheme [3–6] with the so-called artificial antiferromagnetic subsystem (AAF) offers both rigidity of the hard layers and operational temperatures up to 150 °C. In its basic configuration, schematically shown in

0953-8984/00/286217+20$30.00

figure 1(a), the sensor contains two antiferromagnetically coupled layers and one decoupled soft detection layer. Particularly effective is angular position detection with a signal level of 5% and a resolution of about 1°, as shown in figure 1(b).

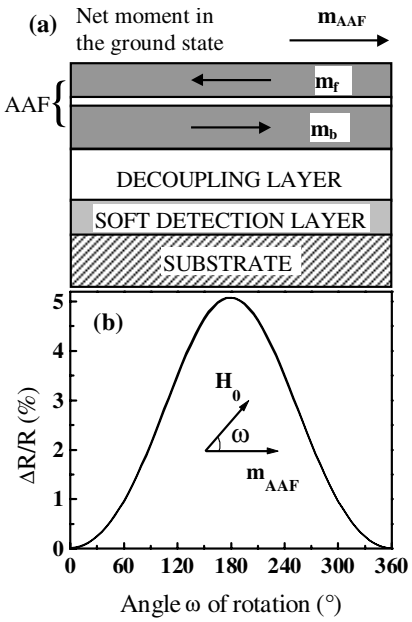

Figure 1. (a) The basic configuration of a sensor with the AAF and (b) its GMR response under the influence of an in-plane rotational field of constant strength 65 Oe for the following stack: Si/SiO_2/Cr 4/Fe 1.5/Co 1/Cu 2.4/Co 2/Cu 0.9/Co 1.2 nm. m_b and m_f are the moments in the so-called bias and flux conducting layers, respectively. The arrow labelled m_{AAF} shows the direction of the AAF's net moment in the case of $m_b > m_f$. Under the influence of the rotational field, the moment of the soft decoupled magnetic layer makes an angle ω with m_{AAF}, whose direction is fixed. This scheme permits 180° resolution. Two orthogonally biased sensors can cover 360°.

The Co–Cu systems are widely used in GMR sensors because of their high magnetoresistivity level. Sensors containing the AAF require perfect AF alignment of the magnetizations right from the first Cu layer in the stack. However, the observation of incomplete AF alignment in the Co–Cu system has often been reported [7–11]. Bridges leading to direct coupling between the magnetic layers or roughness-producing fluctuations between AF and ferromagnetic coupling are often suggested to be responsible for this. The defects are attributed to the non-layer-by-layer growth mode of Co over Cu [12, 13]. Complete AF alignment can nevertheless be achieved by better control of the growth parameters. Recently, we demonstrated that the use of an adequate buffer stack [14] leads to the amount of remanence being negligible. Another way to obtain a complete AF coupling at zero field is by the use of surfactants [15, 16].

The knowledge of the magnetic microstructure, when aiming at producing stable sensors, is of great importance. Many techniques, like Kerr microscopy [17], Lorentz transmission electron microscopy [18, 19], the Bitter pattern technique [20, 21] and polarized neutron reflectivity [22], enable the observation of the domains or domain walls in GMR systems. Barkhausen noise measurements [23] have shown that in Co–Cu multilayers the domains are relatively small when reducing the field from saturation, while they grow after reversing the field direction. It has been confirmed that in ($Co/Ni_{80}Fe_{20}$/Cu) multilayers [18] the domain characteristic sizes depend on the magnetic history of the sample.

In this paper, we report on irreversible domain-phase transformations in AF coupled polycrystalline Co/Cu/Co sandwiches at the first peak in the coupling oscillation. After a brief description of the preparation, the main structural characteristics of the samples are presented. Then, we detail how the soft detection layer located in the buffer stack can be used as a tool to judge the quality of the AF coupling. Various causes of remanence are discussed in the next section, which is focused on irreversible magnetic transformations. We attribute the formation of domains to the freedom in the sense of the magnetization's rotation when leaving the saturated state. In the discussion, we compare the characteristics of magnetic ripple in single layers with those of domains in AF coupled systems. Finally, similarities to and differences from the antiphase domain boundaries [24] are discussed.

2. Sample preparation and measurements

The Co/Cu/Co structures presented here were prepared by sputtering on glass or on Si/(0.5 μm)SiO_2 substrates. All of the samples were protected against oxidization by means of a Cu(2 nm)/Cr(2 nm) capping bilayer, unless otherwise specified. The base pressure of the system is about 5×10^{-8} mbar and the sputtering gas is Ar. The Cr, Co and Cu layers are deposited by DC-magnetron sputtering with an Ar-gas pressure of 10^{-2} mbar, while RF-diode sputtering is used for the Fe and $Ni_{80}Fe_{20}$ targets, with an Ar-gas pressure of 5×10^{-3} mbar. The sputtering rates reach about 90 nm min^{-1} for DC-magnetron sputtering and 7.5 nm min^{-1} for RF-diode sputtering. Three types of buffer layer were tested successfully. The buffer of type FE consists of the following stack: Cr(4 nm)/Fe(1.5 nm)/Cu(10 nm). Types CO and PY consist of the following stacks: Cr(4 nm)/Fe(1.5 nm)/M(0.8 nm)/Cu(10 nm) where M corresponds to Co and $Ni_{80}Fe_{20}$, respectively. The role of the 10 nm thick Cu layer is to smooth the buffer and to decouple the soft magnetic layer. In AAF-based sensors, the latter is used as a soft detection layer [3], as shown in figure 1. The designation of the buffer types FE, CO, PY defined above refers to the nature of the layer lying just beneath the 10 nm thick Cu layer, i.e. Fe, Co, $Ni_{80}Fe_{20}$, respectively.

The magnetoresistance measurements were performed at room temperature by the standard four-point method, with the sensing current perpendicular to the applied field. The magnetization curves were measured by a vibrating-sample magnetometer (VSM) or an alternating-gradient field magnetometer (AGFM) at room temperature. No dead layer could be detected in single Co layers embedded in Cu layers and the Co saturation magnetization reaches 1346 ± 10 emu cm^{-3}, which is close to the value for bulk fcc Co (1449 emu cm^{-3}).

3. Structural characteristics

Both the structural quality of the layers and the morphology of the interfaces are decisive as regards obtaining an AF coupling free of defects. Even ultrahigh-vacuum-evaporated Co/Cu/Co sandwiches with high hcp crystallinity of the Co layers can exhibit intermixed interfaces causing significant remanence and strong thermal variation of the exchange-coupling strength [11].

High-angle x-ray diffraction investigation of Co/Cu structures deposited on the type of buffer FE, i.e. Cr(4 nm)/Fe(1.5 nm)/Cu(10 nm), indicates that the Cr and Fe layers grow mainly in the bcc (110) direction, while the Co and Cu layers are mainly fcc (111) textured. In contrast, when a pure Fe buffer is used, the x-ray diffraction indicates the (100) texture for Fe, which leads to (100) texture for Co and Cu. The stabilization of the (110)-oriented Fe grains is clearly favoured by the Cr seed layer. The (110) texture is of particularly great advantage when Fe

is used in a magnetic sensor and serves as a soft detection layer, since the coercive field is appreciably reduced. Upon coating the detection layer with Co (0.5 nm) in order to increase the GMR signal of the sensor, the coercive fields reach 17.5 Oe and 5 Oe for deposition on the pure Fe (6 nm) and on the Cr(4 nm)/Fe(1.5 nm) buffer layer, respectively.

Transmission electron microscopy has been performed on samples containing an AAF. The electron spectroscopy imaging (ESI) pictures show that the individual layers are continuous. The Fresnel fringes obtained at the Co/Cu interfaces are well resolved and evidence flat interfaces.

Atomic force microscopy measurement was performed *ex situ*. For this experiment, the Co(1.2 nm)/Cu(0.9 nm)/Co(1.2 nm) sandwich was covered with a thin Rh layer, whose surface exposed to air remains free of oxidation. The typical RMS roughness is of the order of 0.3 nm. This is even lower than the typical RMS roughness of the glass or Si/SiO_2 substrate before deposition.

The structural properties of our samples are very satisfactory and constitute an excellent basis for generating an exchange coupling free of defects.

4. Coupling quality

As indicators for the quality of the AF coupling, we consider its strength, its completeness and its distribution [10]. These properties are closely related to the structural quality of the layers and interfaces.

4.1. Buffer layers

An ≈6 nm Fe layer is adequate for growing Co/Cu multilayers with excellent magnetoresistive properties on [9,25]. Nevertheless, because of the magnetic contribution of Fe, the estimation of the amount of remanent magnetization in the Co/Cu system itself is made difficult, especially in the case of a Co/Cu/Co sandwich with thin Co layers. Although the magnetic signal of the Fe layer can in principle be easily evaluated separately, difficulties are encountered when subtracting from the total magnetization the signal of the separately grown Fe layer. This arises from the fact that the signal of this layer, in particular its coercivity, is affected by the stack grown on top. Stresses, orange peel, residual exchange coupling, etc, hinder an independent treatment of the two magnetic contributions.

Therefore, attempts have been made to grow Co(1.2 nm)/Cu/Co(1.2 nm) sandwiches at the first AF maximum in the coupling oscillation on non-magnetic buffer layers. Pure Cu buffer layers (≈6 nm) are hardly suited for achieving AF coupling without coupling defects [25]. Notwithstanding significant improvement when the sandwich is deposited on an ≈30 nm thick Cu layer, the remanent magnetization still reaches one third of the saturation magnetization. Moreover, the thick Cu layer produces a large short circuit, significantly reducing the GMR signal. Although Cr exhibits many crystallographic similarities to Fe, a pure 6 nm Cr buffer layer causes the AF coupling between the Co layers to vanish completely, even when a relatively thick (10 nm) Cu layer is put on top. This may be due to very substantial surface roughness. To smooth the surface of the Cr layer, chosen to be 4 nm thick, we cover it with a 1.5 nm Fe layer. Finally, a 10 nm thick Cu layer is added, which acts as an exchange-decoupling layer between the buffer stack and the Co/Cu/Co sandwich, referred to as the AAF. Therefore, we employed transport measurements and the interaction between the AAF and the detection layer for assessing the amount of remanence in the AAF.

This type of buffer stack, designated as FE, makes it possible to obtain an AAF with very satisfactory magnetoresistive properties, as can be seen in figure 2. The AF coupling

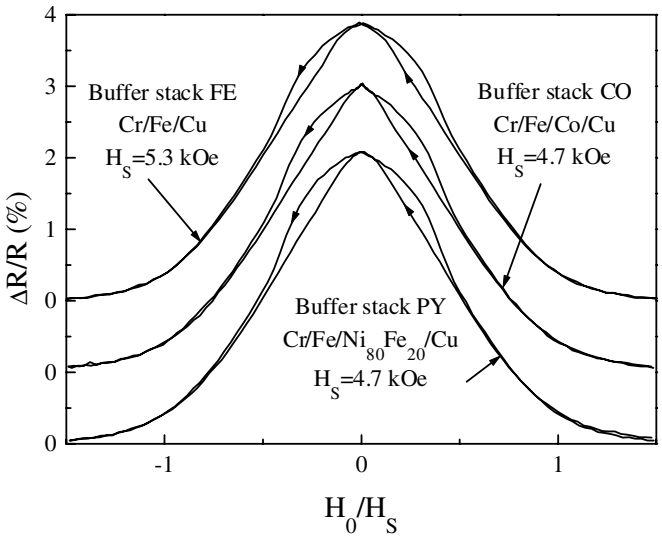

Figure 2. The magnetoresistance curves at room temperature of the AAF Co(1.2 nm)/Cu(0.83 nm)/Co(1.2 nm) deposited on three different types of buffer stack, namely: FE = Cr(4 nm)/Fe(1.5 nm)/Cu(10 nm); CO = Cr(4 nm)/Fe(1.5 nm)/Co(0.8 nm)/Cu(10 nm); PY = Cr(4 nm)/Fe(1.5 nm)/$Ni_{80}Fe_{20}$(0.8 nm)/Cu(10 nm). The applied field H_0 is normalized to the saturation field H_S, defined as the field at which the magnetoresistance has dropped by 90%. Glass substrates are used.

strength J_{AF} reaches 0.43 erg cm^{-2} at room temperature, as deduced from the saturation field ($H_S = 5.3$ kOe) using the relation

$$J_{AF} = \frac{H_S M_S t_{\mathrm{Co}}}{2} \tag{1}$$

where M_S is the magnetization of Co layers at saturation ($M_S = 1346$ emu cm^{-3}) and t_{Co} is the thickness of one Co layer ($t_{\mathrm{Co}} = 1.2$ nm). As far as Co/Cu/Co sputtered sandwiches are concerned, J_{AF} is remarkably large, indicating the high structural quality of the layers. The buffer types CO and PY, which are obtained by inserting a 0.8 nm Co and a 0.8 nm $Ni_{80}Fe_{20}$ layer between the Fe and the Cu layers, respectively, are also well suited for growing high-quality Co/Cu/Co sandwiches, as shown in figure 2. The coupling strength is of the same order of magnitude, and these types of buffer are characterized by excellent reproducibility.

While an ≈6 nm Fe buffer layer is often mentioned in the literature as leading to an excellent quality of the AF coupling in the case of a Co/Cu/Co sandwich, we have been able to reduce, in comparison, the magnetic contribution of the buffer by about a factor of four. Since the Fe is deposited by RF-diode sputtering, i.e. at a very low rate, the deposition time for the complete stack is reduced by more than a factor of two. On the other hand, the Fe is characterized by very high resistivity, which means that the mean free path is also small in the majority channel, and increasing the thickness of the Fe layers above 1.5 nm does not give rise to any significant increment in the GMR signal.

4.2. Completeness of the coupling

In the case of sandwiches with thin magnetic layers, it is still difficult to judge from the magnetization curves whether the observed remanence is caused by the contribution of the magnetic layer in the buffer stack alone. Let us now describe how this soft magnetic layer

influences the magnetoresistive measurements, and how the remanence of the AAF can be deduced from the magnetoresistance curve.

The total change in the stack resistance is due to both the change in the mutual orientation of the magnetization in the AAF and that in the orientation in the detection layer with respect to the AAF layers. Figure 3 provides these theoretical data for the contribution of the different layers to the GMR signal, while the detection layer–AAF interaction is varied by changing the thickness of the Cu layer. The stack considered is as follows: Co 3 nm (detection layer)/Cu 0.5–10 nm (decoupler)/Co 1.5 nm/Cu 0.9 nm/Co 1 nm. We took a pure Co detection layer because we have previously determined experimentally the mean free path for the minority and majority electrons. Three different situations are compared: firstly, the switching of the AAF while the detection and the middle magnetic layer remain in the reference direction (curve 1); secondly, the switching of the detection layer while both the Ms of both AAF layers keep the reference direction (curve 2); and, finally, the simultaneous switching of the AAF and the detection layer while the middle magnetic layer remains in the reference direction (upper curve 3). These plots show that, to a good approximation, curve 3 for the two layers switching can be found by simply adding the changes caused by the single-layer switching of curves 1 and 2, i.e. by superposing the AAF signal and the detection layer signal. For more detailed calculations, see reference [26].

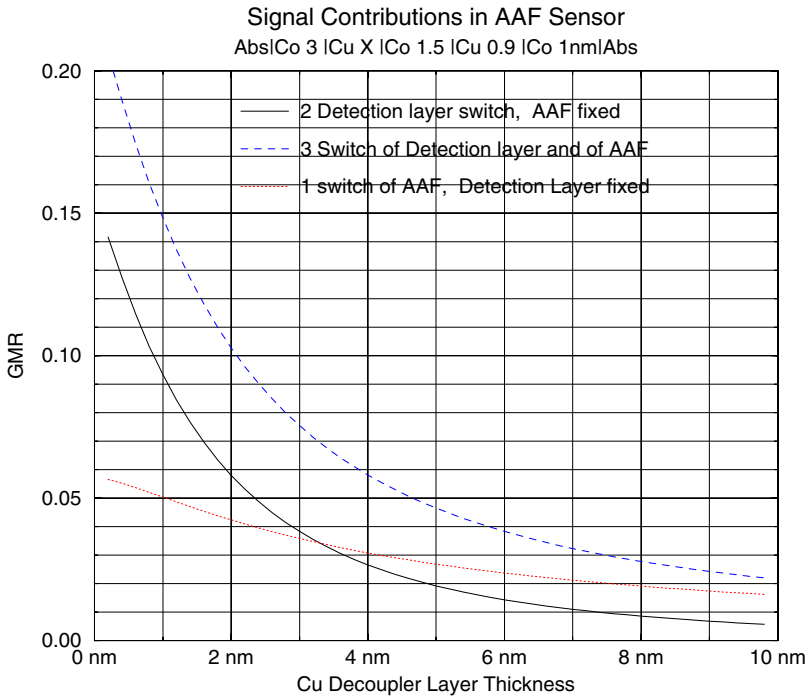

Figure 3. Theoretical data on the contribution of the different layers to the GMR signal when the detection layer–AAF interaction is varied by changing the thickness of the Cu layer. The stack considered is as follows: Co 3 nm (detection layer)/Cu 0.5–10 nm (decoupler)/Co 1.5/Cu 0.9/Co 1 nm (AAF). Three different situations are compared: first, the switching of the AAF while the detection layer and the middle magnetic layer remain in the reference direction (curve 1); second, the switching of the detection layer while both the Ms of both AAF layers keep the reference direction (curve 2); and, finally, the simultaneous switching of the AAF and the detection layer while the middle magnetic layer remains in the reference direction (upper curve 3).

First we shall consider the behaviour of an ideal isolated AF coupled system after saturation in the positive direction. Upon reducing H_0, the moments $\boldsymbol{m}_1$ and $\boldsymbol{m}_2$ of the two magnetic layers (with the same modulus m) make angles of φ_1 and φ_2, respectively, with the positive direction, as indicated at the top of figure 4. The angles φ_1 and φ_2 have the same absolute value φ, which increases continuously between 0 and 90° as H_0 is reduced from H_S to 0. The angle φ satisfies $\cos\varphi = H_0/H_S$ for $H_0 < H_S$, and the component of the isolated AAF's moment in the positive direction satisfies $2mH_0/H_S$, as represented by the full line in figure 4(a). It is well established [27] that the $R(H_0)$ characteristic for perfectly AF coupled layers is quadratic, so the normalized GMR signal of the AAF is the parabola

$$\Delta R_{\mathrm{AAF}}(H_0) = 1 - \cos^2\varphi = 1 - (H_0/H_S)^2$$

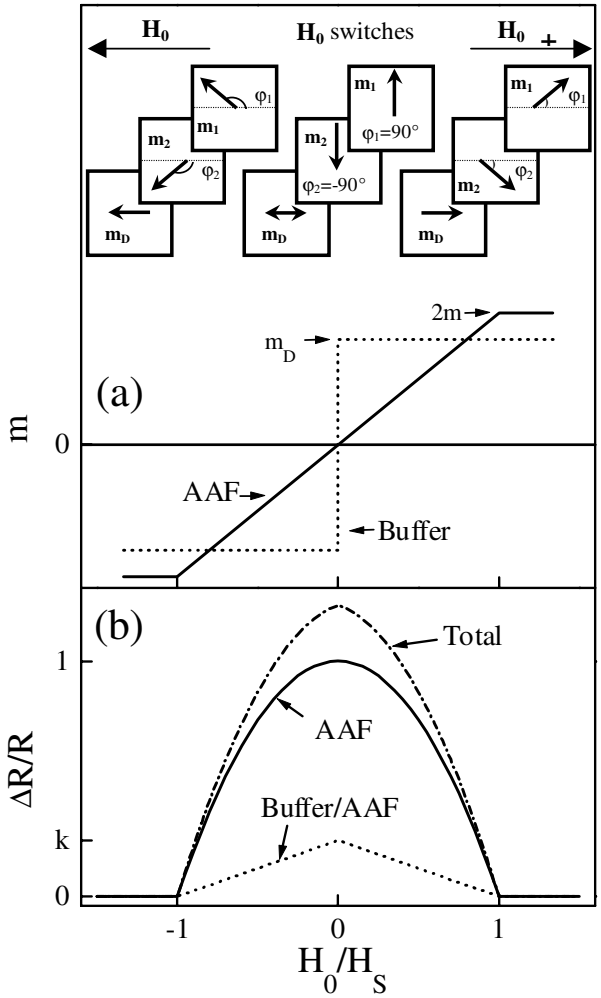

Figure 4. Stylized $m(H_0)$ and $\Delta R/R(H_0)$ curves. In (a), the full line corresponds to the response of the isolated AF coupled system and the dotted line to the soft magnetic layer. In (b), the full line is $\Delta R_{\mathrm{AAF}}(H_0)$, the dotted line is $\Delta R_{\mathrm{INT}}(H_0)$ and the dot–dashed line is their superposition. At the top, $\boldsymbol{m}_1$ and $\boldsymbol{m}_2$ represent the moments within the AF coupled system and $\boldsymbol{m}_D$ the moment in the soft magnetic layer. Note the perpendicular orientation of the magnetizations within the AAF at zero field, relative to the positive direction.

(the full line in figure 4(b)). Let us now consider the interaction between the AF coupled system and the magnetic layer of the buffer stack with moment $\boldsymbol{m}_D$, supposed to have an ideal soft-magnetic stepwise response (the dotted line in figure 4(a)). As H_0 is reduced from H_S to 0, $\boldsymbol{m}_D$ remains aligned in the positive direction, so the absolute value of the angle between $\boldsymbol{m}_D$ and $\boldsymbol{m}_1$ ($\boldsymbol{m}_2$) is φ. The GMR signal resulting form this interaction is known [27] to vary linearly with $\cos\varphi$. Therefore, the GMR signal resulting from this interaction is roughly given by $\Delta R_{\mathrm{INT}}(H_0) = k(1 - H_0/H_S)$ for $H_0 < H_S$ (the dotted line in figure 4(b)), where k is the ratio of the level of this interaction to the level of the signal of the AAF and corresponds to the rotation of the detection layer from 0 to 90°, and adds to $\Delta R_{\mathrm{AAF}}(H_0)$, so the total GMR signal is modified (the dot–dashed line in figure 4(b)). The slope of this curve at $H_0 = 0$ is related to the magnitude of $\Delta R_{\mathrm{INT}}(H_0)$. This simple model applies well if one considers the upper branches of the magnetoresistance curves of figure 2. For each type of buffer used, the GMR signal is the superposition of a parabolic curve and a triangular one. As will be discussed in section 5, these branches correspond to a magnetic state that is much closer to the ideal case than the ones to which the lower branches correspond.

Let us now consider the case of a small lag $\Delta\varphi$, for example due to resistive forces against moment rotation, in the magnetic response of the AAF. Such resistive forces are typical for polycrystalline films, in which the anisotropy axes are usually randomly distributed. Upon rotation of the magnetization by the field, it has to overcome energy barriers at which energy is lost and where it is lagging behind the field. $\Delta\varphi$ is then responsible for a small non-zero component in the positive direction at $H_0 = 0$. The absolute value of the angle between $\boldsymbol{m}_1$ ($\boldsymbol{m}_2$) and $\boldsymbol{H}_0$ becomes $\varphi = \arccos(H_0/H_S) - \Delta\varphi$ for $H_0 < H_S$. The response $\Delta R_{\mathrm{AAF}}(H_0)$ deviates by $2\,\Delta\varphi \sin 2\varphi$ from the ideal parabolic signal and is most sensitive to this modification for φ-values around 45°. In contrast, the signal is not sensitive to the deviation from the complete antiparallel alignment of the AAF at zero field, i.e. to the remanence caused by the small lag. On the other hand, $\Delta R_{\mathrm{INT}}(H_0)$ deviates by $k\,\Delta\varphi \sin\varphi$ from the perfect triangular signal, which is most disturbed for φ-values around 90°, which means at zero field. Upon switching of the soft magnetic layer, a sudden jump of $2k\,\Delta\varphi$ will occur in the total GMR signal. The factor 2 arises from the fact that the change in angle between the positive direction and $\boldsymbol{m}_D$ reaches 180°. $\Delta\varphi$ in this example might originate in homogeneous friction of the AAF. It is obvious that any other cause of remanence in the AAF will produce a similar effect.

4.3. The maximum signal of the detection layers

Raising the question of the determination of the maximum possible jump in the GMR upon switching of the soft detection layer is in order. This maximum jump would be detected if $\boldsymbol{m}_1$ and $\boldsymbol{m}_2$ were to be 'pinned' in the positive direction at $H_0 = 0$. In this case, upon switching of $\boldsymbol{H}_0$, the change of angle between $\boldsymbol{m}_D$ and $\boldsymbol{m}_1$ ($\boldsymbol{m}_2$) would be of 180°, giving rise to a jump of $2k$ in the GMR. This is twice the level k of the interaction between the perfect AAF and $\boldsymbol{m}_D$ represented in figure 4(b), since there, the relative angle varied continuously between 0 and 90° only. To obtain the desired fixing of $\boldsymbol{m}_1$ and $\boldsymbol{m}_2$ in the positive direction, the following layer sequence is prepared: Co(1 nm)/Cu(0.5 nm)/Co(1 nm)/Cu(0.83 nm)/Co(1 nm). The Cu(0.5 nm) layers couple ferromagnetically to the two first Co layers in order to attach $\boldsymbol{m}_1$ and $\boldsymbol{m}_2$ together. The second Cu(0.83 nm) layer ensures AF coupling between this pair and the third Co layer in order to 'pin' the pair in the positive direction. The total friction against rotation of the subsystem's magnetization is increased [3] by about a factor of 3 compared to that for a single magnetic layer with the same total Co thickness (3 nm). The coercivity can originate from several physical mechanisms: the blocking phenomenon related to the in-plane anisotropy ripple in polycrystalline films, friction of domain-wall motion, etc. It is

essential to note that in the ground state at zero field, the magnetic moments of the first pair are aligned antiparallel to the third Co layer and lie in the positive direction. This is schematically represented by the arrows in figure 5. The extra magnetic layer does not significantly contribute to the GMR interaction with the detection layer, so the maximum jump at zero field, $2k$, will be approximately reproduced.

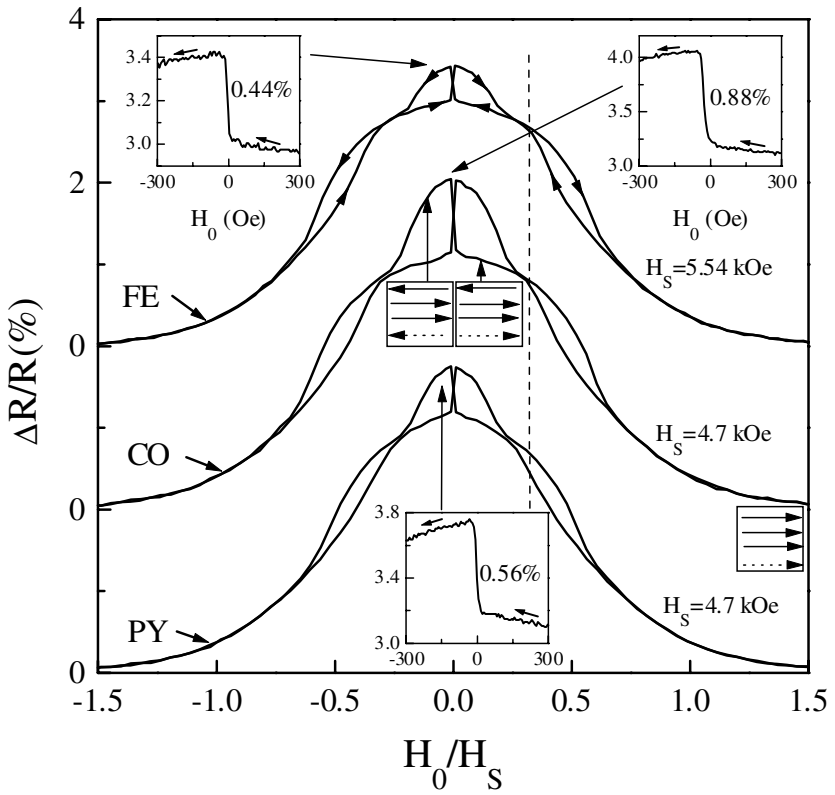

Figure 5. The magnetoresistance curve at room temperature of the AAF Co(1 nm)/Cu(0.5 nm)/Co(1 nm)/Cu(0.83 nm)/Co(1 nm) deposited on three different types of buffer stack. The arrows in the boxes represent the magnetic moments as functions of the field. The dashed arrow corresponds to the soft magnetic layer's moment, and the full arrows to the moments of the Co layers in the AAF. The insets detail the GMR response upon switching of the soft detection layer in the buffer stack. Glass substrates are used.

A plateau in the magnetization curve, and consequently in the GMR curve, corresponding to the regime with opposite alignment of the moments, is predicted [3] at $H_P = H_S/3$. It is clearly recognizable in figure 5, which presents the GMR signal as a function of the normalized field H_0/H_S for the sample Co(1 nm)/Cu(0.5 nm)/Co(1 nm)/Cu(0.83 nm)/Co(1 nm) deposited on each type of buffer. The dashed vertical line at $H_0/H_S = 1/3$ corresponds well to the occurrence of the plateau, especially in the case of deposition on the type FE and CO buffer stacks.

Choosing three different buffer stacks allows the interaction between the soft magnetic layer and the subsystem to be modified. The level of the interaction is determined by the electron scattering events of both spin-current channels at the different interfaces and also in the bulk of the magnetic materials. Upon switching of the soft detection layer, the plateau in figure 5 is followed by a sudden step near zero field, with the magnitudes of 0.44%, 0.88%

and 0.56% for the buffer types FE, CO and PY, respectively. This agrees well with the fact that the GMR ratio is much larger for Co/Cu multilayers than for $Ni_{80}Fe_{20}$/Cu and Fe/Cu multilayers.

We have argued in subsection 4.2 that a small stepwise increase in the GMR signal is expected to occur upon switching of the soft magnetic layer when an AF coupled symmetrical sandwich shows remanence. In the specially designed subsystem presented just above, the jump detected around roughly zero field is the GMR increase that would be observed if the sandwich had 100% remanence. Assuming that steps of 0.025% can easily be detected in the magnetoresistance curves, this means that the relative remanences amounting roughly to 6%, 3% and 4.5% can be easily recognized in the GMR signal of an AF coupled system deposited on type FE, CO and PY buffers, respectively.

4.4. Remanence of the AAF on various buffers

The GMR signal of the symmetrical AAF Co(1.2 nm)/Cu(0.83 nm)/Co(1.2 nm) presented in figure 2 has been carefully measured between 150 Oe and −150 Oe, after saturation at 10 kOe. The signal of the sample, deposited on each type of buffer, is detailed in figures 6(a), 6(b), 6(c) for decreasing applied fields only. To find out at which field the detection layer switches, the buffer stacks of type FE, CO, PY have been prepared separately with no AAF on top. The coercive fields have been determined by a VSM, and the loops are shown in figures 6(d), 6(e) and 6(f). In figure 6(a), no change at all is observed in the GMR signal upon switching the soft magnetic layer of type FE. One can conclude that the net moment of the AAF at $H_C = -8$ Oe is less than 6% of the saturation moment. In figure 6(b), a sudden drop of the GMR signal is seen at $H_C = -45$ Oe, the switching field of the soft magnetic layer of type CO. Nevertheless the resistivity value is reduced upon soft magnetic layer reversal, which means that the net moment of the AAF had already changed sign. In figure 6(c), no signal modification is clearly

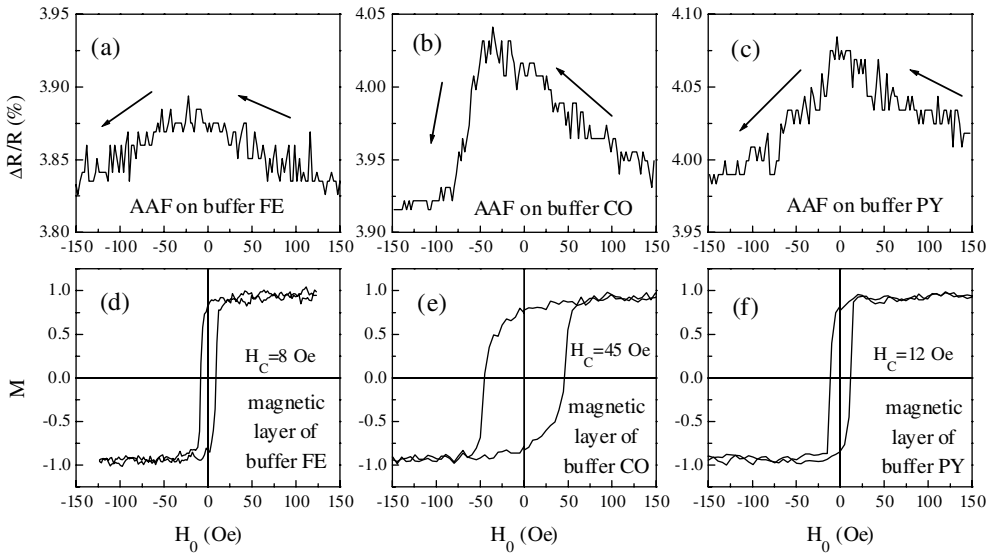

Figure 6. The low-field GMR response (first row) of the Co(1.2 nm)/Cu(0.83 nm)/Co(1.2 nm) AAF deposited on a buffer stack of type (a) FE, (b) CO, (c) PY; and magnetization loops (second row) of the separately deposited buffer stacks of type (d) FE, (e) CO and (f) PY. The magnetization loops permit determination of the switching field of the soft magnetic layer included in the buffer.

identified at $H_C = -12$ Oe, the switching field of the soft magnetic layer in type of buffer PY. The remanence of the AAF is less than 4.5%.

In these three samples, no remanence could be detected. Since each system contains only one Co/Cu/Co sandwich, it proves that each of the buffer stacks provides samples with a high quality of the AF coupling. Let us now show that it is possible to detect some small amount of remanence by the method presented in subsection 4.2. Figure 7 shows the GMR signal of an AAF deposited on a type CO buffer stack, and the substrate used now consists of Si/SiO_2 instead of glass. Around zero field, a sudden increase in the GMR signal is clearly detected. The inset details the jump, which occurs around $H_0 = -45$ Oe, i.e. the switching field of the soft layer in the type CO buffer stack. While the sample deposited on glass (see figure 2 and figure 6(a)) has no detectable remanence, the same sample deposited on Si/SiO_2 clearly shows a small amount of remanence. This does not necessarily point to a small fraction of coupling defects, such as pinholes, leading to areas with parallel alignment of the magnetization. It may indicate the existence of the Néel type of domain walls, as will be discussed below.

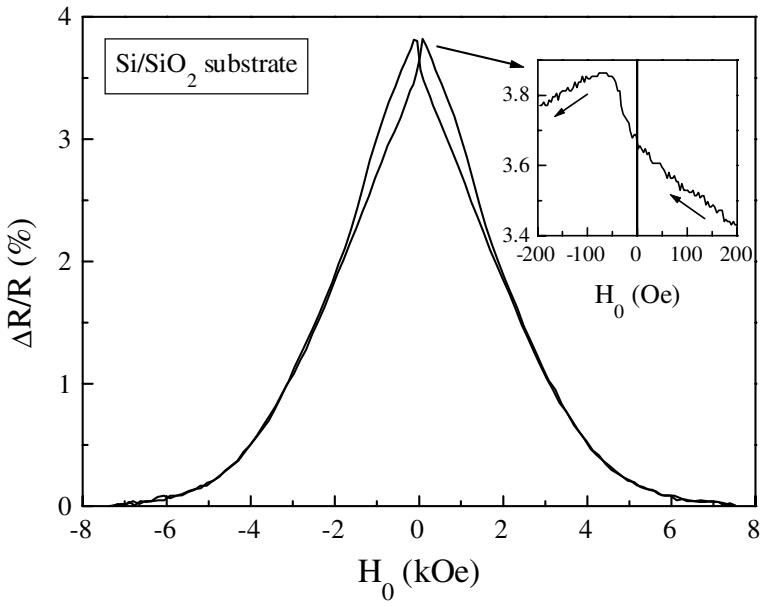

Figure 7. The magnetoresistance curve at room temperature of the AAF Co(1.2 nm)/Cu(0.83 nm)/Co(1.2 nm) deposited on the type of buffer CO. A Si/SiO_2 substrate is used. Note the difference between the GMR response at low field of this AAF and of the same AAF prepared on a glass substrate (see figure 6(b)).

5. Irreversible transitions

The GMR curves presented in section 4 all exhibit clear hysteretic behaviour. To clarify the origin of the differences between the branches, the magnetoresistance and the magnetization have been measured along minor loops. The minor loops start at positive saturation, then the applied field H_0 is reduced to a minimum value H_{rev}, which can be either positive or negative, and finally, H_0 is increased again toward positive saturation. The major loop corresponds to a complete hysteresis cycle.

5.1. Positive reversal field H_{rev}

Five minor loops with H_{rev}-values between 713 Oe and 1.21 kOe are presented in figure 8(a). The minor loops with $H_{\mathrm{rev}} = 1.21$ kOe and $H_{\mathrm{rev}} = 1.06$ kOe are fully reversible, as recognized from the fact that their $R(H_0)$ branches both coincide with the lower $R(H_0)$ branch of the major loop. For $H_{\mathrm{rev}} = 962$ Oe, an irreversible process starts to occur: the return branch (i.e. that for increasing applied field) starts to split up from the one with the lowest $R(H_0)$ values. This means that 962 Oe is just below the threshold value H_{T1} at which irreversible changes start to take place. Upon further reducing H_{rev} to well below H_{T1}, the irreversibility becomes more and more pronounced; see for example the minor loops with $H_{\mathrm{rev}} = 894$ Oe and $H_{\mathrm{rev}} = 713$ Oe in figure 8(a).

The magnetization of this sample has been measured along five minor loops as shown in figure 8(b). The major loop also presents hysteretic behaviour. The branch with the highest mean magnetization $M(H_0)$ along the applied field forms the pendant to the branch of the GMR curve with the lowest $R(H_0)$ signal, while the branch with the lowest $M(H_0)$ is the counterpart of the GMR branch with the highest $R(H_0)$. The minor loops with $H_{\mathrm{rev}} = 1.436$ kOe and $H_{\mathrm{rev}} = 1.030$ kOe are fully reversible. Obviously, upon further reducing H_{rev}, an irreversible process takes place, as shown by the minor loop with $H_{\mathrm{rev}} = 926$ Oe in figure 8(b). The $M(H_0)$ level of the return path lies slightly below the $M(H_0)$ level of the branch with decreasing field. For H_{rev}-values smaller than the transition field value $H_{\mathrm{T1}} = 926$ Oe, the irreversibility becomes more and more apparent, as for example for $H_{\mathrm{rev}} = 821$ Oe and $H_{\mathrm{rev}} = 622$ Oe.

Of course, the values of the transition field H_{T1} found by GMR and AGFM measurements, 962 Oe and 926 Oe respectively, are not exact and the real H_{T1} is somewhat larger, because at these fields, the irreversibility can already be clearly distinguished. In fact the measured H_{T1} depends on the sensitivity of the detection method. This may be a reason for the discrepancy between the two measured values.

5.1.1. Development of the domain structure. Now we shall delve deeper into the origin of the observed irreversibility. Macroscopically, our samples are isotropic because of their polycrystalline nature in which the preferential axes of the crystallites are randomly oriented. Since no effective anisotropy is present in our systems, we believe that the irreversibility in the GMR and $M(H_0)$ signals, in the present structure, can be attributed to a domain-phase-transformation process. The domain configuration develops when leaving the parallel state at saturation. Ideally, the magnetization inside each Co layer would start to rotate uniformly and reach the perfect AF alignment at zero field, with both magnetization vectors perpendicular to the original saturation field (see $\boldsymbol{m}_1$ and $\boldsymbol{m}_2$ in figure 3(a)). The polycrystalline character of our Co layers originates in the amorphous nature of the SiO_2 substrate. As a consequence, there is no macroscopic anisotropy, and no unique sense of the rotation of the magnetization in a given layer is imposed. As is known from ripple theory, the lateral coherence of the dipoles is limited, so dipoles that are far apart, i.e. at distances larger than the lateral coherence length L, can rotate independently. Therefore, half of the moments inside the crystallites will rotate clockwise and half will rotate anticlockwise in a specific layer. This results in the formation of magnetic domain structures that are the counterparts of the well known ripple structures in single films. Inhomogeneities may add to the thermal activation and facilitate the local rotation of the moments. For example, stepwise variations in the spacer thickness produce inhomogeneities in the coupling distribution, so the rotation starts at different fields at different positions. This hinders a rotation in unison with the layer's magnetization. Upon reducing H_0, the moments inside the areas presenting the strongest coupling should rotate first. At isolated nucleation sites, the sense of the rotation of the moments is free, and probably some

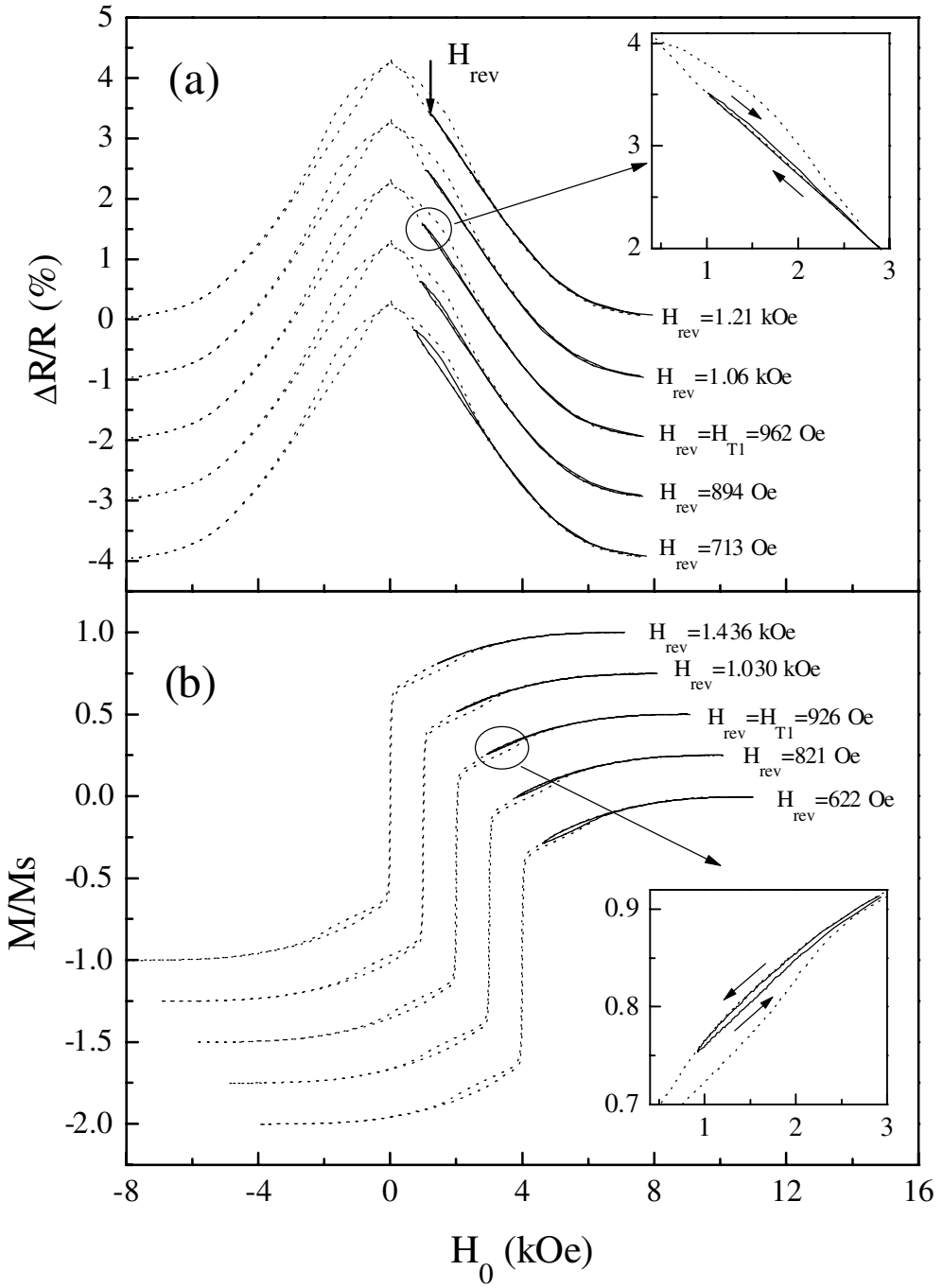

Figure 8. The (a) magnetoresistance and (b) magnetization minor loops with positive values of H_{rev} for the AAF Co(1.2 nm)/Cu(0.83 nm)/Co(1.2 nm) deposited on the type CO of buffer stack. Each of the minor loops is superposed for comparison on the major loop. The inset details in each case the irreversibility due to domain-phase transformations at the field H_{T1}. In (a) the vertical scale is common to all curves, shifted by 1% for clarity. In (b) both vertical and horizontal scales are common, shifted by 0.5 and 1 kOe respectively, for clarity.

small differences in the local anisotropy energies between the crystallites of the two magnetic layers determine the local sense of the rotation. Sites at which the moments in one specific Co layer rotate clockwise or anticlockwise are distributed over the surface of the sample.

Upon reducing H_0 further, the magnetizations inside the areas with weaker AF coupling also rotate. Here, the sense of the rotation may be imposed by neighbouring regions in which the sense of the rotation is already established, or is defined by the local forces when such regions are far away compared to the lateral exchange coherence length [10] L:

$$L \approx \sqrt{\frac{-dA}{J_{AF}}} \approx 5 \text{ to } 10 \text{ nm} \tag{2}$$

where d is the magnetic layer thickness, A is the bulk exchange constant and J_{AF} is the AF coupling strength. Finally, more and more moments rotate and domain walls with the Néel type of structure are created when domains with different senses of rotation of the magnetization in a given Co layer meet.

5.1.2. Annihilation of the domain structure. We will now return to the domain conversion process. As long as the wall angles are small enough, the configuration with a high density of domains remains stable and the wall angles can vary in a reversible fashion. This is the case for the fully reversible minor loops of figures 8(a) and 8(b). Upon lowering the field, the domain-wall angles increase and so the wall energy density does too. On reducing H_0 below a certain threshold value, the presence of domain walls becomes unfavourable. As a consequence, domains will annihilate and cause the separation of the descending- and ascending-field branches in figures 8(a) and 8(b). A further reduction of H_0 makes more and more domains vanish. Finally, the return path of the minor loop reaches the highest branch of the major GMR curve (or the lowest branch of the magnetization curve). This branch is characterized by a low density of domains. When the size of the domains is large enough compared to the electronic mean free path and domain-wall area, the magnetic layers will respond as if they were uniformly magnetized. Consequently, the simple GMR model presented in figure 4(b) fits the branch with the upper $R(H_0)$ curve quite well.

Nevertheless, the agreement is not perfect and the upper GMR curves still deviate from the ideal parabolic shape. Their very long tails evidence lateral interlayer coupling variations, that influence the sizes of the domains and wall angles. The wall energy stored in one of the domain walls created is a function of J_{AF}, of the wall angle α and of A. It can be written as [10]

$$\sqrt{(AJ_{AF})}\, f(\alpha) \tag{3}$$

and increases continuously upon decreasing H_0. It is well known that the pressure of the curved portions [28] will increase. In the case of homogeneous frictional forces, the wall segments with the highest wall energy density and smallest radius of curvature tend to move first. As a consequence, the domains with the smallest lateral dimensions in regions with high AF interlayer coupling are expected to collapse first.

5.2. Negative reversal field H_{rev}

Up to now, we have confined ourselves to irreversible phenomena occurring when coming from saturation. At zero field after positive saturation, we arrive at a similar state with a low density of walls. However, the magnetizations in the adjacent layers are opposite now. Let us now look at the transformations arising from the antiparallel state, by considering the minor loops with H_{rev} taking negative values. Figure 9(a) presents the GMR signal of the AAF measured along

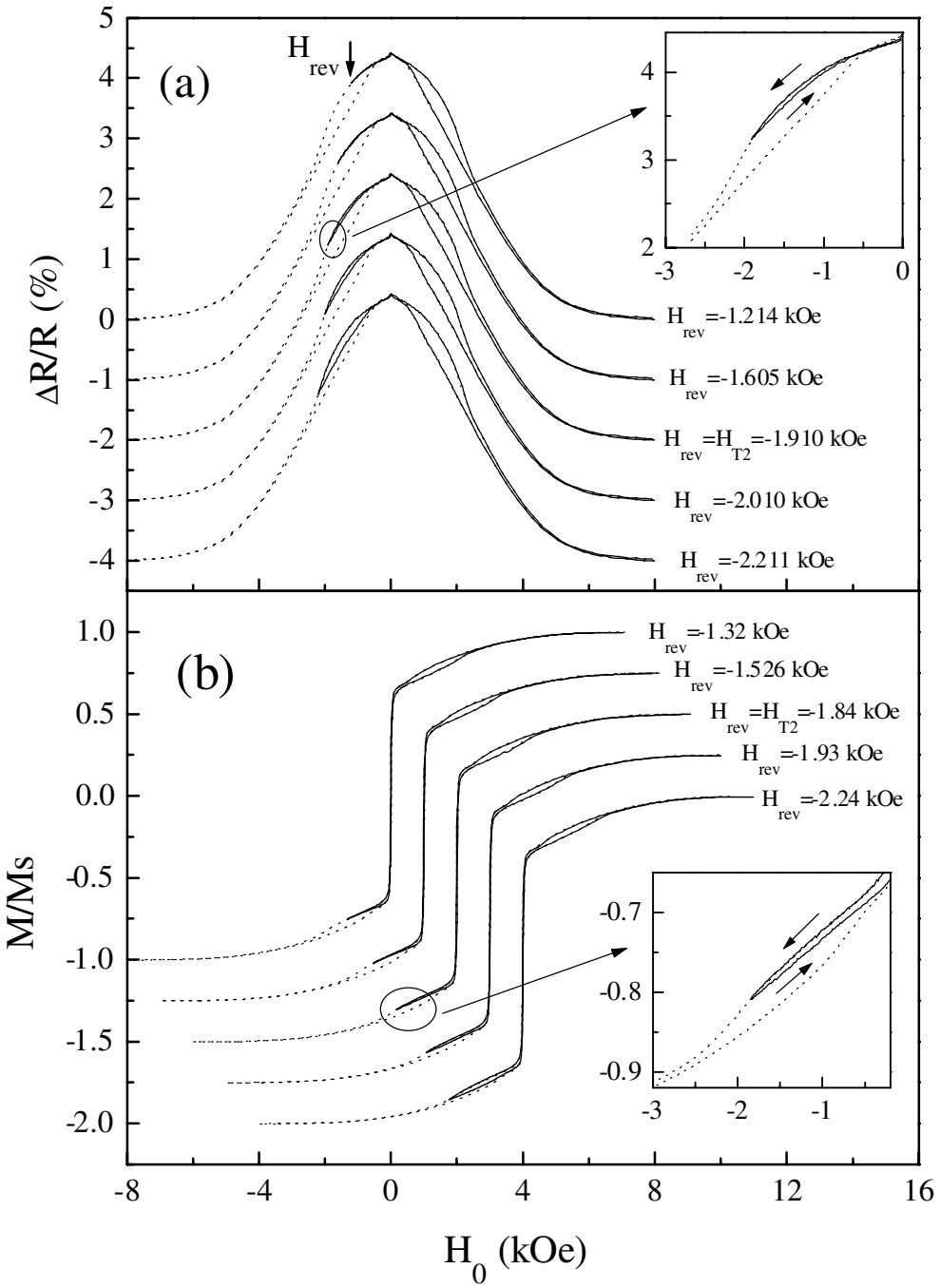

Figure 9. The (a) magnetoresistance and (b) magnetization minor loops with negative values of H_{rev} for the AAF Co(1.2 nm)/Cu(0.83 nm)/Co(1.2 nm) deposited on the type CO of buffer stack. Each of the minor loops is superposed for comparison on the major loop. The inset details in each case the irreversibility due to domain-phase transformations occurring at the field H_{T2}. In (a) the vertical scale is common to all curves, shifted by 1% for clarity. In (b) both vertical and horizontal scales are common, shifted by 0.5 and 1 kOe respectively, for clarity.

five such loops. Our attention here is on the branches where the applied field is only negative. The minor loops with $H_{\text{rev}} = -1.214$ kOe and $H_{\text{rev}} = -1.605$ kOe are fully reversible. Upon further increasing the strength of the applied field in the negative direction, another irreversible process occurs, as is visible for the minor loop with $H_{\text{rev}} = -1.910$ kOe. This indicates that the absolute value of the threshold field H_{T2} for this irreversibility is very close to 1.90 kOe. The irreversibility becomes more and more pronounced for $H_{\text{rev}} = -2.010$ kOe and $H_{\text{rev}} = -2.211$ kOe.

The same phenomenon is observed for the five magnetization minor loops of figure 9(b). The curve for $H_{\text{rev}} = -1.84$ kOe confirms that the absolute value of H_{T2}, the threshold field for irreversibility to occur, is close to 1.90 kOe, as determined from GMR measurement.

Upon increasing the applied field in the negative direction from the AF state, the magnetization inside the large domains is forced to rotate to reach the parallel alignment. As long as no regions have reached this state, no new domains are formed upon a subsequent reduction of the field to zero, because the sense of the rotation with respect to the antiparallel alignment is already defined. The magnetic phase with low domain density is maintained and it is possible to move in a reversible way along the upper branch of the GMR curve (or along the lowest branch of the magnetization curve). However, as soon as the areas with the weakest AF coupling are saturated, domains are likely to be created again upon reducing the strength of the field due to the freedom in the sense of the rotation, as discussed in section 5.1.1 for the descending-field flank.

The threshold field H_{T2} indicates when portions of the sandwich become saturated again. For larger absolute values of H_{rev}, more and more regions are ferromagnetically aligned, according to the interlayer coupling distribution, so more and more domains are created while the return path is being traced out.

6. Discussion

6.1. Ripple configurations in magnetic single thin films

The domain-splitting phenomenon which is the subject of this paper calls to mind the well known ripple configurations in magnetic single thin films [29]. In this case also, a domain structure develops upon reducing the field from saturation. Again, it is created in the incipient phase by the independent rotation of the magnetization from side to side. In general, the effect is strong in polycrystalline films, where the random orientation of the crystallite axes causes a lateral distribution of the direction and strength of the effective anisotropy.

Lateral variations in many physical parameters, such as interlayer coupling, anisotropy and total magnetic moment of both magnetic layers, originating in, e.g., thickness variations, might play a role in the domain formation in the AF coupled sandwiches. However, most of these, like the coupling and magnetic moments, do not lead to a local preference in the rotation sense and are only of secondary importance. Even spatial variation in the effective anisotropy direction is not a sufficient condition for the rotation sense to vary laterally, as is the case for single thin films. In addition, the surface density of the effective anisotropy torque at a given lateral position should be different for the two magnetic layers.

We shall now briefly discuss the size of the domains. In the ripple structure, the transverse coherence length ξ_T, being related to the mean domain size perpendicular to the saturation field, is known to be larger than its longitudinal counterpart ξ_L. Both are proportional to the square root of the effective bulk exchange constant A. ξ_L is further inversely proportional to the square root of the effective mean anisotropy (being typically in the 1 μm range), while ξ_T is relatively large due to the cohesion originating from magnetostatic interactions, the range of

which decreases at decreasing film thicknesses. This already indicates that ξ_T is much smaller as usual, due to the small thicknesses of the present magnetic films. However, the transverse coherence is even more strongly suppressed by the opposite rotation of the moments in adjacent layers, leading to the mutual cancellation of the stray fields from the two layers. The coherence length in AF coupled sandwiches, as given by equation (2), is inversely proportional to the square root of J_{AF} and is in the tens of nanometres range. Therefore, the domain structure is much more dense in the AF coupled sandwiches than it is in the ripple configuration of single thin films. This makes the direct experimental observation of the domains very complicated.

6.2. Virgin curves

In our samples presenting no detectable remanence after reducing the field from saturation to zero, we expect at zero field a magnetic configuration with a very low density of domains. There should be almost no difference between the upper branch of the GMR major loop and the virgin GMR curve, since the magnetic seed layer effect also occurs during the deposition of our samples. The seed layer effect is a consequence of the order of growth. The first-deposited Co layer (the seed layer) of the AAF contains after deposition a small density of domains due to the ferromagnetic nature of that single layer. After that, Cu is deposited with a thickness that couples the Co atoms of the second magnetic layer antiferromagnetically to the first Co layer. In other words, the domain structure in the seed layer will be copied in the second Co layer. This is demonstrated in figure 10(a) for a sample deposited on a glass substrate. The curve labelled 1 corresponds to the virgin GMR curve whereas the curves labelled 2 and 3 are the major loop. The resistance at zero field after cycling is reduced by only 0.04% relative to the resistance in the as-deposited state. Furthermore, the curves labelled 1 and 3 are almost perfectly mirrored. This strongly supports our hypothesis that a great number of domains vanish upon reducing the applied field from saturation, until a state with relatively large domains is reached at $H_0 = 0$. The behaviour is different for a sample with smaller J_{AF} and deposited on Si/SiO_2. As shown in figure 10(b), the relative reduction in resistance after cycling is 0.13%, which points to a non-negligible domain-wall density at zero field. This behaviour agrees well with the considerations developed in section 5.1.2 concerning the influence of J_{AF} on the magnetic domain configuration.

Let us return to the sample presented in figure 7, for which some remanence is detected at the switching field of the detection layer (-45 Oe). Whether the domain walls can overcome the local energy barriers, which lie at the origin of the frictional forces, and collapse depends on the local coupling strength, i.e. on the wall energy. Possibly, at zero field enough regions persisted with weak coupling, such that the domain walls could not collapse, for a detectable remanence to be still visible.

7. Conclusions

We have studied the domain-phase transformations occurring in AF coupled sandwiches. Buffer stacks containing the Cr/Fe bilayer are very well suited for depositing high-quality samples with (111) texture of the sputtered Co–Cu layers. In the best samples, the coupling strength is larger than 0.4 erg cm^{-2}. A method was presented that allows one to judge the completeness of the AF coupling in sandwiches. It consists in observing the height of the jump in the GMR response that occurs upon switching the soft magnetic layer included in the buffer stack. Special samples containing the artificial antiferromagnetic subsystem have been designed that enable correlation of this height with the amount of remanent magnetization. It is possible to obtain Co/Cu/Co sandwiches at the first maximum in the coupling oscillation

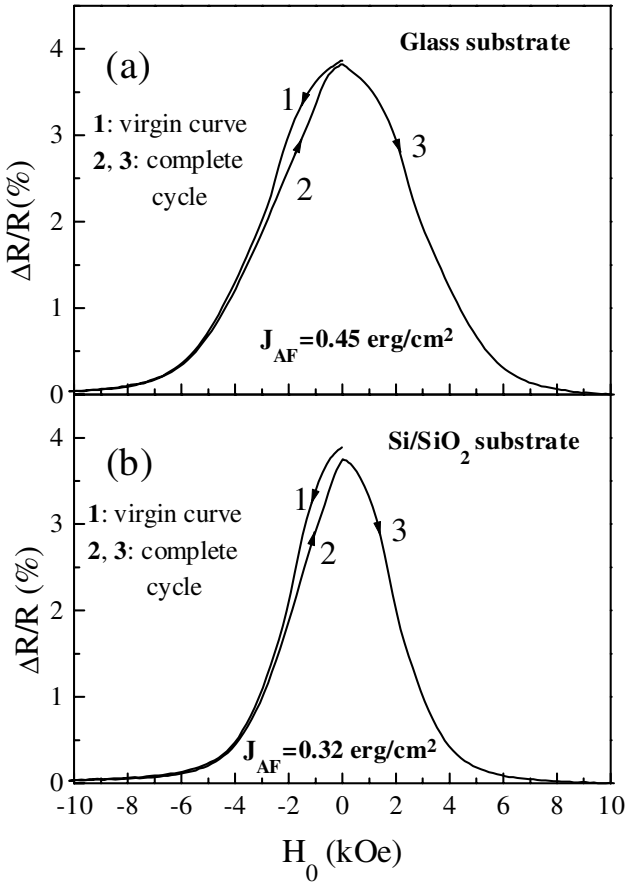

Figure 10. The magnetoresistance at room temperature of the AAF (a) Co(1.2 nm)/Cu(0.83 nm)/Co(1.2 nm) and (b) Co(1.2 nm)/Cu(0.9 nm)/Co(1.2 nm) deposited on the buffer stack of type FE. In (b), the coupling strength is weaker than in (a) due to a slightly thicker Cu coupling layer. The reduction relatively to the as-deposited state of the sample's resistance after cycling is 0.04% and 0.13% in cases (a) and (b), respectively. In (b), a non-negligible domain-wall density exists at zero field after cycling.

without detectable remanence by use of an adequate buffer. Nevertheless, for some samples, remanence is detected. This is possibly related to the significant presence of domain walls at zero field. Domains are created upon reducing the field from the saturated state, due to the freedom in the sense of the magnetization's rotation. The irreversibilities observed in GMR and magnetization curves are attributed to domain-phase conversion. Small differences in the coupling distribution function between samples are possible. In some cases, the annihilation is almost complete and no remanence is detected. In other samples, domain walls, still present at zero field, lie at the origin of non-negligible remanence. These hypotheses are supported by comparing the resistance at zero field in the as-deposited state and after cycling.

Acknowledgments

This work was partly supported by the Brite Euram 'Contactless position sensors based on new GMR multilayer materials'. We thank our colleagues from Siemens and IPCMS for technical

assistance and fruitful discussions: G Gieres, K H Rojek, H Mai for the sample preparation, G Rupp for magneto-transport measurements, K Cherifi-Khodjaoui for x-ray diffraction, H Cerva for TEM, and K Ounadjela, M Demand and C Tiusan for AFM measurement.

References

[1] Kergoat R, Miltat J, Valet T and Jérome R 1994 *J. Appl. Phys.* **76** 7087
[2] Dieny B, Speriosu V S, Parkin S S P, Gurney B A, Wilhoit D R and Mauri D 1991 *Phys. Rev.* B **43** 1297
[3] van den Berg H A M, Clemens W, Gieres G, Rupp G, Schelter W and Vieth M 1996 *IEEE Trans. Magn.* **32** 4624
van den Berg H A M, Clemens W, Gieres G, Rupp G, Vieth M, Wecker J and Zoll S 1997 *J. Magn. Magn. Mater.* **165** 524
Clemens W, van den Berg H A M, Rupp G, Schelter W, Vieth M and Wecker J 1997 *J. Appl. Phys.* **81** 4310
[4] Leal J L and Kryder M H 1998 *J. Appl. Phys.* **83** 3720
[5] Huai Y, Zhang J, Anderson G W, Rana P, Funada S, Hung C Y, Zhao M and Tran S 1999 *J. Appl. Phys.* **85** 5528
[6] Tiusan C, Dimopoulos T, Ounadjela K, Hehn M, van den Berg H A M, da Costa V and Henry H 2000 *Phys. Rev.* B **61** 580
[7] Highmore R J, Shih W C, Somekh R E and Evetts J E 1992 *J. Magn. Magn. Mater.* **116** 249
[8] Schreyer A, Bröhl K, Ankner J F, Majkrzak C F, Zeidler Th, Bödeker P, Metoki N and Zabel H 1993 *Phys. Rev.* B **47** 15 334
[9] Rupp G and Schuster K 1993 *J. Magn. Magn. Mater.* **121** 416
Rupp G and van den Berg H A M 1993 *IEEE Trans. Magn.* **29** 3102
van den Berg H A M and Rupp G 1994 *IEEE Trans. Magn.* **30** 809
[10] van den Berg H A M and Schmeusser S 1993 *IEEE Trans. Magn.* **29** 3099
van den Berg H A M 1997 *Magnetic Thin Films and Multilayer Systems: Physics, Analysis and Industrial Applications* ed U Hartmann (Berlin: Springer)
van den Berg H A M, Wecker J and Schewe H 1994 *Curr. Top. Magn. Reson.* **1** 235
[11] Persat N, Dinia A, Jay J P, Mény C and Panissod P 1996 *J. Magn. Magn. Mater.* **164** 37
Persat N and Dinia A 1997 *Phys. Rev.* B **56** 2676
[12] de la Figuera J, Prieto J E, Ocal C and Miranda R 1993 *Phys. Rev.* B **47** 13 043
[13] Castañer R, Prieto C, de Andrés A, Martínez J L, Trigo J and Sanz J M 1996 *Solid State Commun.* **98** 179
[14] Persat N, van den Berg H A M and Dinia A 1997 *J. Magn. Magn. Mater.* **165** 446
Persat N, van den Berg H A M, Cherifi-Khodjaoui K and Dinia A 1997 *J. Appl. Phys.* **81** 4748
[15] Camarero J, Spendeler L, Schmidt G, Heinz K, de Miguel J J and Miranda R 1994 *Phys. Rev. Lett.* **73** 2448
Camarero J, Graf T, de Miguel J J, Miranda R, Kuch W, Zharnikov M, Dittschar A, Schneider C M and Kirschner J 1996 *Phys. Rev. Lett.* **76** 4428
Kuch W, Dittschar A, Lin M T, Salvietti M, Zharnikov M, Schneider C M, Kirschner J, Camarero J, de Miguel J J and Miranda R 1997 *J. Magn. Magn. Mater.* **170** L13
[16] Egelhoff W F Jr, Chen P J, Powell C J, Stiles M D, McMichael R D, Lin C L, Sivertsen J M, Judy J H, Takano K and Berkowitz A E 1996 *J. Appl. Phys.* **80** 5183
Chopra H D, Hockey B J, Chen P J, Egelhoff W F Jr, Wuttig M and Hua S Z 1997 *Phys. Rev.* B **55** 8390
[17] Schäfer R, Hubert A and Parkin S S P 1993 *IEEE Trans. Magn.* **29** 2738
[18] Heyderman L J, Chapman J N and Parkin S S P 1994 *J. Phys. D: Appl. Phys.* **27** 881
Heyderman L J, Chapman J N and Parkin S S P 1994 *J. Appl. Phys.* **76** 6613
[19] Zimmerman T, Zweck J and Hoffmann H 1995 *J. Magn. Magn. Mater.* **149** 409
[20] Gijs M A M, Giesbers J B, Beliën P, van Est J W, Briaire J and Vandamme L K J 1997 *J. Magn. Magn. Mater.* **165** 360
[21] Hua S Z, Lashmore D S, Swartzendruber L J, Egelhoff W F Jr, Raj K and Chopra H D 1997 *J. Appl. Phys.* **81** 4582
[22] Borchers J A, Gehring P M, Erwin R W, Ankner J F, Majkrzak C F, Hylton T L, Coffey K R, Coffey M A, Parker M A and Howard J K 1996 *Phys. Rev.* B **54** 9870
Borchers J A, Dura J A, Majkrzak C F, Hsu S Y, Loloee R, Bass J and Pratt W P Jr 1998 *Proc. 7th Joint MMM–Intermag Conf.*
[23] Hardner H T, Weissman M B, Salamon M B and Parkin S S P 1993 *Phys. Rev.* B **48** 16 156
Hardner H T, Parkin S S P, Weissman M B, Salamon M B and Kita E 1994 *J. Appl. Phys.* **75** 6531
Hardner H T, Weissman M B and Parkin S S P 1995 *Appl. Phys. Lett.* **67** 1938
Hardner H T, Weissman M B, Miller B, Loloee R and Parkin S S P 1996 *J. Appl. Phys.* **79** 7751
[24] Highmore R J, Somekh R E, Shih W C, McLoughlin I M and Evetts J E 1993 *Appl. Surf. Sci.* **65/66** 124

[25] Parkin S S P, Bhadra R and Roche K P 1991 *Phys. Rev. Lett.* **66** 2152
[26] Dieny B, Li M, Liao S H, Horng C and Ju K 2000 *J. Appl. Phys.* **87** 3415
[27] Dieny B 1994 *J. Magn. Magn. Mater.* **136** 335
[28] Chikazumi S 1964 *Physics of Magnetism* (New York: Wiley)
[29] Fuller H W and Hale M E 1960 *J. Appl. Phys.* **31** 238